Nanoscale Res Lett (2007) 2:175–183
DOI 10.1007/s11671-007-9050-z

NANO EXPRESS

Photochemically reduced polyoxometalate assisted generation of silver and gold nanoparticles in composite films: a single step route

Sangaraju Shanmugam · Balasubramanian Viswanathan · Thirukkallam K. Varadarajan

Published online: 13 March 2007

Abstract A simple method to embed noble metal (Ag, Au) nanoparticles in organic–inorganic nanocomposite films by single step method is described. This is accomplished by the assistance of Keggin ions present in the composite film. The photochemically reduced composite film has served both as a reducing agent and host for the metal nanoparticles in a single process. The embedded metal nanoparticles in composites film have been characterized by UV–Visible, TEM, EDAX, XPS techniques. Particles of less than 20 nm were readily embedded using the described approach, and monodisperse nanoparticles were obtained under optimized conditions. The fluorescence experiments showed that embedded Ag and Au nanoparticles are responsible for fluorescence emissions. The described method is facile and simple, and provides a simple potential route to fabricate self-standing noble metal embedded composite films.

Keywords Polyoxometalates · Organic–inorganic nanocomposite · Silver · Gold · Fluorescence

Introduction

In recent years the synthesis and characterization of nanoparticles have received attention because of their distinctive properties and potential uses in various fields like microelectronics [1], photocatalysis [2], magnetic devices [3] and powder metallurgy [4]. The intrinsic properties of a metal nanoparticle are mainly determined by size, shape, composition, crystallinity, and morphology [5]. A number of methods have been developed to prepare noble metal colloids, such as chemical reduction with or without stabilizing agents [6], photochemical reduction [7], microwave [8], sonochemical [9], and radiochemical methods [10]. To realize the potentialities of noble metal nanoparticles in technological and biological applications, they should entrapped/embedded in polymer matrix and made into thin films or scaffolds. Fabrication of such type of hybrid systems consisting of metal nanoparticles and organic polymers is of considerable interest because these materials exhibit novel properties.

Direct synthesis of nanoparticles in solid matrices is attracting increasing interest in terms of practical applications and synthetic challenges. Because these materials exhibit novel combinations of metal particle and polymer properties that are attractive for applications in nonlinear optics [11], photo imaging and patterning [12], glazing elements for sunlight control and magnetic devices [13, 14], sensor fabrication [15], antimicrobial coatings [16], and catalysis [17]. The dispersed metal nanoparticles into polymers in non-aggregated form, with small diameters allow the preparation of materials with reduced light characteristic properties for applications as optical filters, linear polarizers, and optical sensors. Therefore the size, shape, and spatial distribution are important to have modulated optical properties of final composite material. Several approaches have been reported to embed the noble metal nanoparticles in various matrices such as silica, alumina, borate glass, and MgO by sputtering, ion implantation, thermal vapor deposition, physical vapor deposition, and radio frequency magnetron co-sputtering [18]. All these methods require tedious procedures to adopt. So it is necessary to develop an easy and simple

S. Shanmugam · B. Viswanathan (✉) ·
T. K. Varadarajan
Department of Chemistry, Indian Institute of Technology Madras, Chennai 600 036, India
e-mail: bvnathan@iitm.ac.in

method to embed metal nanoparticles in matrices. We have used a strategy wherein the active components (polyoxometalates) have been used to prepare composites consisting organic (PVA) and inorganic (SiO_2) components. The composite film has been used to reduce the noble metal ions and also used as matrix to embed the metal nanoparticles produced in a single step.

Polyoxometalates (POM) are metal oxide clusters, discrete and well defined at atomic level with extensive structures and properties [19]. Among the numerous polyoxometalates that exist, Keggin type polyoxometalates are studied extensively, because of their easy preparation, and rich redox properties [20]. The redox properties can be manipulated by proper substitutions in addenda, or hetero atoms [21]. The Keggin ions can undergo stepwise multielectron redox process electrochemically, photochemically, and radiolytically, without any structural modifications. Troupis et al. have employed polyoxometalates ($SiW_{12}O_{40}^{4-}$, $PW_{12}O_{40}^{3-}$) as photocatalysts and stabilizers to prepare noble metal nanoparticles in homogeneous medium [22]. Recently, Sastry et al. employed Keggin ions as UV-switch able reducing agents for the synthesis of Au–Ag core shell nanoparticles and gold nanosheets in aqueous solutions [23]. We have reported the preparation of Pt/C using organic–inorganic nano composite wherein the composite acts as a nanoreactor for deposition of anisotropic Pt nanoparticles on carbon [24].

In the present investigation, we have employed polyoxometalate embedded organic–inorganic nanocomposite film as reductant and as well as the host for the generation of Ag and Au nanoparticles prepared by a simple chemical route. The present study is mainly concentrated on the formation of Ag and Au nanoparticles on organic-inorganic nanocomposite films. The formation of metal nanoparticles was characterized with various physicochemical techniques. As such no reports are available at present for embedding the Ag and Au nanoparticles in organic–inorganic nanocomposite by this strategy. The presence of metal nanoparticles in composite film was characterized by UV–Visible, TEM, EDAX and XPS techniques. The size and density of metal nanoparticles were controlled by adjusting the reaction parameters such as concentration of metal precursor and time of dipping. A narrow size distribution of metal nanoparticles was observed. The embedded metal nanoparticles exhibit fluorescence emission.

Experimental

Materials

Silicotungstic acid (SiW) and Polyvinylalchol (PVA) (72000) were purchased from Sisco Research Laboratories Pvt. Ltd., and Tetraethylorthosilicate was purchased from E-Merck. All other chemicals were reagent grades and were used as received.

Preparation of composite

The organic–inorganic composite was prepared by the following method. Polyvinylalcohol (PVA) dissolved in deionized water was stirred in an oil bath for 10 min, to which tetraethylorthosilicate and silicotungstic acid solutions were slowly added and refluxed at 353 K for 6 h. For a typical synthesis, to a solution of PVA (30 wt% in water) was added a solution containing 20 wt% tetraethyl orthosilicate and 50 wt% silicotungstic acid. The resultant solution was refluxed at 353 K for 6 h, to obtain a clear viscous gel. The final transparent solution was used to make films for further studies. The polyoxometalate was entrapped into the polymer matrix by interacting with the hydroxyl groups of polymer. The polyoxometalate ($H_4SiW_{12}O_{40}$) acts as an acid catalyst for the hydrolysis and promotes the condensation of the tetraethyl orthosilicate present in the precursor. The crosslinking between the silica matrix and polyvinyl alcohol takes place in presence of POM.

Structural characterization

UV–VIS spectra of materials were recorded on Cary 5E UV-VIS-NIR spectrophotometer. The microscopic images of the samples were taken with Philips CM12/STEM scientific and analytical equipment. TEM sampling grids were prepared by mounting the composite film on a carbon-coated grid. The electron diffraction pattern was obtained by using the same instrument. The accelerated voltage was 120 kV and the focal length was 50 cm. A gold single crystal was used as a standard to check the camera length. XPS measurements were performed in ultrahigh vacuum (UHV) with Kato, axis HS monochromatized Al Kα cathode source, at 75–150 W, using low energy electron plod gun for charge neutralization. Survey and high resolution individual metal emissions were taken at medium resolution, with pass energy of 80 eV, and step of 50 meV. X-ray diffraction studies were recorded on a Bruker AXS D advance powder diffractometer with a Cu Kα (α = 1.5418 Å). The room temperature photoluminescence excitation and emission spectra were recorded for the powder samples using a Jobin Yvon Fluorolog-3-11 spectrofluorometer.

Electrochemical characterization

A single glass compartment cell three electrode was employed for the cyclic voltammetry and chronoamperometry studies. Pt wire and Saturated Calomel Electrode

(SCE) were used as counter and reference electrode, respectively. A 0.076 cm^2 area glass carbon (GC) served as the working electrode. The electrochemical studies were carried with a potentiostat/Galvanostat Model 273 A. The glassy carbon was first polished with alumina paste (procured from BAS, USA) followed by ultrasonication in water for 5 min and then polished with diamond paste (3 μm dia) and again ultrasonicated for 10 min in water. The composite was coated on glassy carbon electrode by taking 10 μL of PVA–SiO_2–SiW composite and dried in an oven at 80 °C for 2 min to get a thin film on glassy carbon electrode (PVA–SiO_2–SiW/GC). The electrolyte was degassed with nitrogen gas before the electrochemical measurements.

Results and discussion

The composite film was coated on quartz plate for absorption study. The photoreduction of nanocomposite film was monitored through UV-Visible spectroscopy; because of the reduced silicotungstic acid has a characteristic absorption band in visible region. Reduced silicotungstic acid showed an absorption peak around 750 nm indicating the formation of single electron reduced silicotungstate ion. Figure 1 shows the UV–Visible spectra of reduced composite at various time intervals. The intensity of 750 band increased with an increase in the time of irradiation indicating that more silicotunsgstic acid is getting reduced. Up to 60 min, there is an increase in the intensity, but after 60 min, there is no change in the absorption band (750 nm) indicating that all the silicotungstate ions in the composite have been completely reduced. The formation of reduced silicotungstic acid was further confirmed by ESR studies. It is observed that the ESR spectra of photoreduced composite film exhibited a signal at $g = 1.813$ at 77 K, which is originating from the d^1(W) electrons of reduced species present in the composite (single electron reduced species $SiW_{12}O_{40}^{5-}$, $SiW_{12}O_{40}^{4-} \rightarrow SiW_{12}O_{40}^{5-}$) [25]. The reduced composite film can be re-oxidized by exposing to oxygen or any other oxidizing atmosphere. The reduced composite film is stable (retains blue color) for longer time when it is stored in an inert atmosphere. Thus the reduced composite was employed as reducing medium as well as host for the formation of metal nanoparticles. This reaction is a solid–liquid type electron transfer reaction. The reduced composite film can be able to transfer electrons to the metal ions, which are present in the aqueous solution. So, this reaction is heterogeneous in nature. TEM studies of organic–inorganic composite revealed that the $SiW_{12}O_{40}^{4-}$ ions are homogeneously dispersed and the resulted composite is homogeneous [26].

The thickness of the reduced composite film is about 50 micron. When the composite coated glass plate was dipped into 20 mM of aqueous silver nitrate solution, it was observed that the blue color has changed into golden yellow within a few minutes time indicating the formation of silver nanoparticles in the composite film (inset c in Fig. 2). The reduced composite film exhibited two broad bands at 460 and 750 nm (Fig. 2, curve b). When the reduced composite film was dipped into $AgNO_3$, these bands disappeared and a new band at 420 nm is observed indicating the formation of Ag nanoparticles in the composite film [27] (Fig. 2, curve c). The Ag embedded composite film can be removed from the substrate by peeling off, thus the self-standing film was synthesized. Similarly, the reduced composite film is dipped into the $HAuCO_4$ solution for 30 min, the blue color film changed into pink-violet color (inset d in Fig. 2). The pink–violet

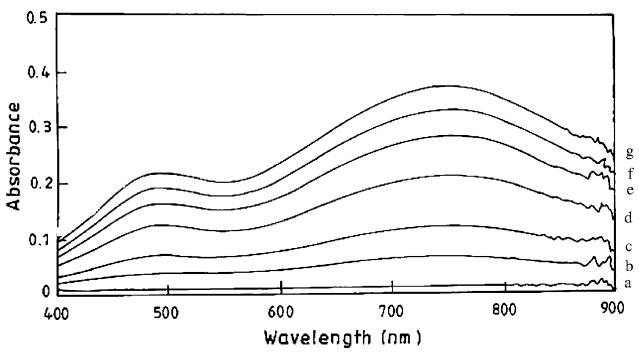

Fig. 1 UV–Visible spectra of composite film under sun light irridiation at various time intervals. (**a**) 0 min, (**b**) 5 min, (**c**) 10 min, (**d**) 15 min, (**e**) 20 min, (**f**) 25 min, and (**g**) 30 min

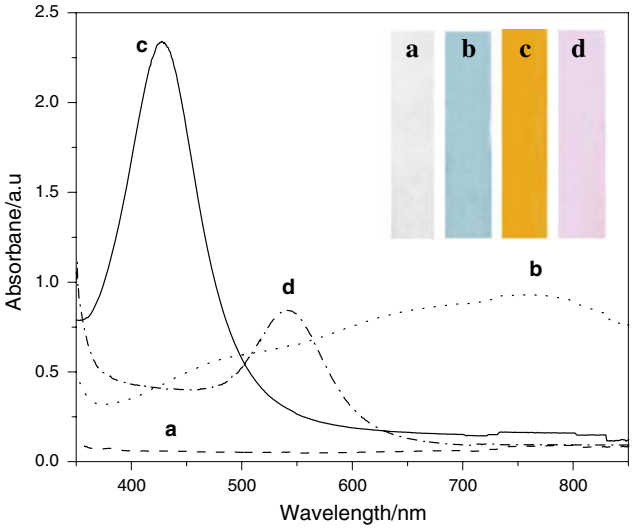

Fig. 2 Absorption spectra of nanoparticles embedded in composite films (**a**) $SiW_{12}O_{40}^{4-}$ (**b**) reduced $SiW_{12}O_{40}^{5-}$ (**c**) Ag and (**d**) Au. Inset shows photo image of the self-standing composite films

composite film exhibited a band at 520 nm, characteristic of Au nanoparticles [28]. These observations clearly demonstrate that the reduced composite film was able to reduce metal ions into metal nanoparticles, which is evidenced from the surface plasmon bands of Ag, Au nanoparticles.

The time evolution formation of Ag nanoparticles in the composite film was monitored by UV-Visible spectroscopy. As the time of dipping increased, the blue color of the film gradually changed to yellow within a minute and the intensity of the color increased which is evidenced from Fig. 3. The corresponding absorption spectrum is shown in Fig. 4. A red shift of the surface plasmon band of Ag nanoparticles is evident from Fig. 4, with a concomitant peak broadening when dipping time was increased from 5 to 30 min. The shift to the higher wavelength and broadening of the surface plasmon absorption band upon incorporation of silver in the composite film is induced by the change in dielectric constant of the environment around the Ag nanoparticles [29]. The particle size can be controlled by choosing suitable dipping time intervals and concentration of metal ions solutions. As the concentration of $AgNO_3$ is increased, the intensity of the surface plasmon band increases and the absorption shifts to higher wavelength. The red shift and broadening of the surface plasmon band is due to the change in dielectric constant and also the increase in particle size, polydispersity and amount of metal nanoparticles in composite film. From the absorption spectra (Fig. 4), it is evidenced from full-width at half-maximum (FWHM), the particle size is increased as the dipping time increased [29]. The FWHM of the surface plasmon band has increased from 74 to 112 nm as the dipping time has increased from 5 to 30 min. And also, the increase in the surface plasmon band intensity indicates the increase in amount of metal nanoparticles in composite film. Figure 5 shows the TEM images of reduced composite films for various time intervals in $AgNO_3$ solution. Further, as the dipping time increased (5, 10, 30 min) the

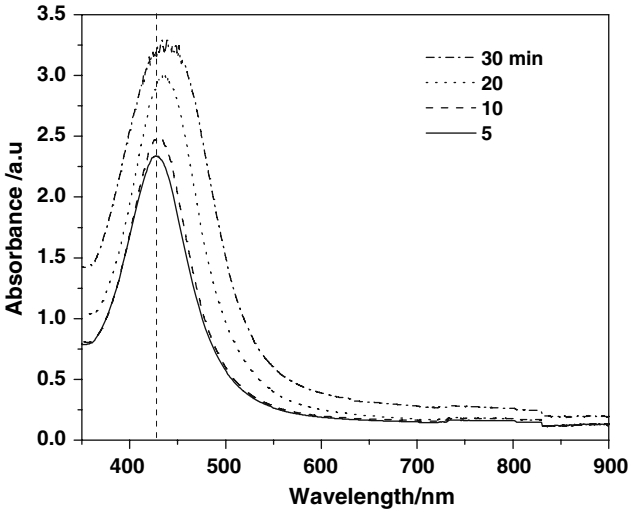

Fig. 4 UV–Visible spectra of Ag embedded composite film at different dipping time intervals

average particle size has increased (9, 15, 19 nm) and also the population of silver nanoparticles. It is also clear from the TEM images that the dipping time increases, the Ag nanoparticles population increases. The composite dipped for 30 min is highly populated and well dispersed all over the composite (Fig. 5c). From the electron diffraction pattern of Ag nanoparticles composite film (Fig. 5d), a clear ring pattern, the lattice parameter was calculated to be 0.411 nm. This is in good agreement with that of bulk metallic Ag (a_0 = 0.408 nm; JCPDS File No.4-0784). The average particle size of Ag was found to be 19 ± 2 nm for 30 min dipping. The size of Ag nanoparticles can be varied in the composite by adjusting the concentration of $AgNO_3$, and also as demonstrated by varying the dipping time. The EDX measurements have been carried using a nano beam. The EDX spectrum of individual Ag nanoparticles from the composite film is presented in Fig. 5e, which indicates the presence of metallic Ag nanoparticles. Figure 5f shows the XRD pattern of composite dipped for 30 min

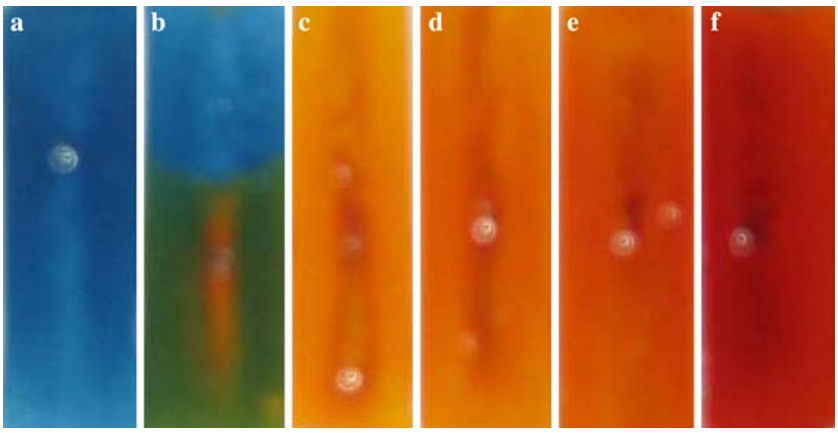

Fig. 3 Photograph of formation of Ag nanoparticles in composite film at different dipping time intervals, $AgNO_3$ - 20 mM, (**a**) 0 min, (**b**) 1 min, (**c**) 5 min, (**d**) 10 min, (**e**) 20 min, (**f**) 30 min

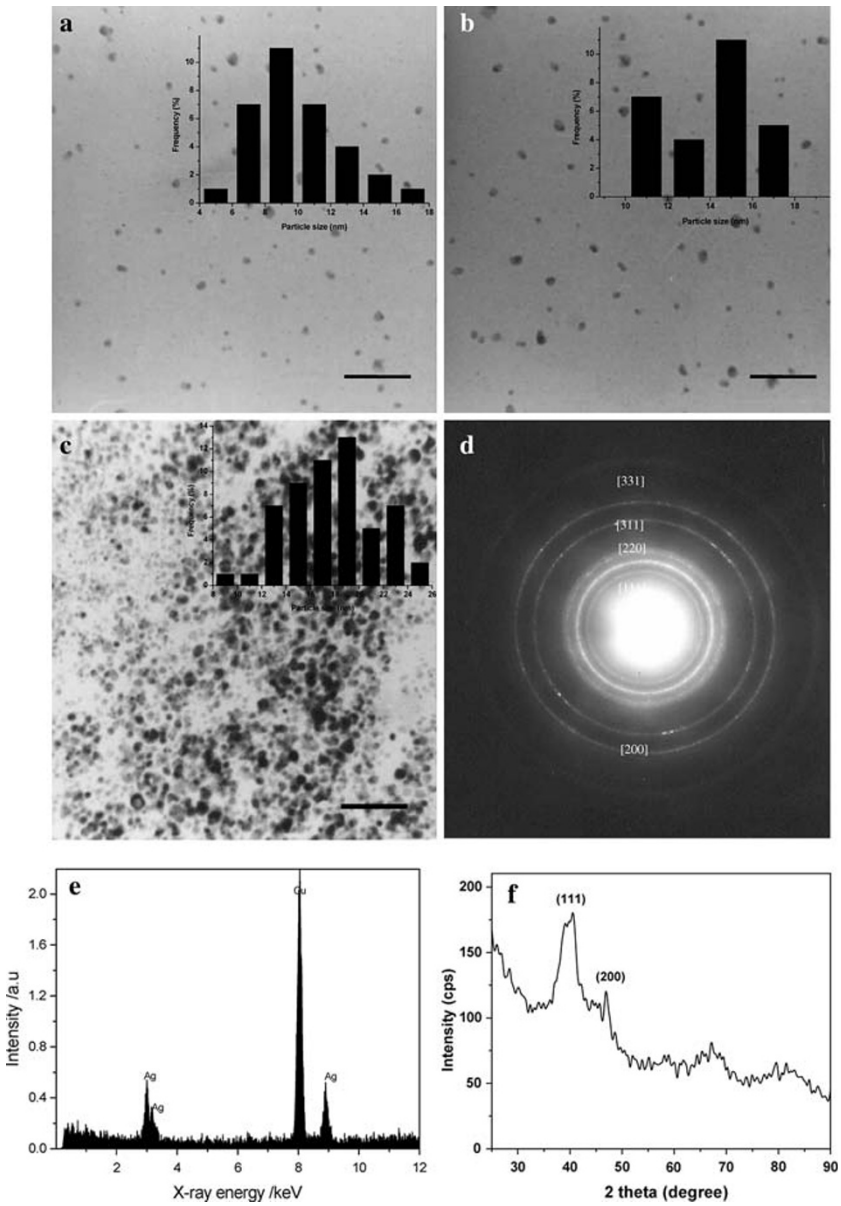

Fig. 5 TEM images of silver nanoparticles embedded composite at different dipping time intervals in 20 mM of $AgNO_3$ (**a**) 5 (**b**) 10 (**c**) 30 and (**d**) selected area diffraction pattern (**e**) EDX spectra of (**c**) and (**f**) XRD pattern of composite film dipped for 30 min. Inset shows corresponding histograms. Scale bar: 100 nm

indicating the presence of metallic Ag nanoparticles. The strongest XRD peak corresponds to Ag (111) diffraction and also a less intense peak also observed (2θ = 44.4°) due to Ag (200) diffraction. The XRD measurement showed the composite consisting of metallic Ag without any AgO.

TEM images of Au nanoparticles of 3.3 and 5.4 mM $HAuCl_4$ solutions for a dipping time of 30 min are shown in Fig. 6. The particle size as well as the amount of Au in the composite is found to increase with the increase in the concentration of $HAuCl_4$ solution. The change in the color of the film (blue to pink) after 10 min dipping and the characteristic surface plasmon band at 546 nm indicate the formation of the Au nanoparticles in the composite film. The TEM images of reduced composite dipped for 30 min 3.3 mM $HAuCL_4$ and 5.4 mM $HAuCl_4$ are presented in Fig. 6a and b. The average Au particle size is 9 ± 3 and 15 ± 2 nm for 3.3 and 5.4 mM $HAuCl_4$, respectively. The formation of highly distributed Au nanoparticles in the composite film with spherical shape is evidenced from the TEM studies.

The presence of Ag and Au in composite films was further characterized with XPS spectroscopy. Figure 7a shows the XPS survey spectra of Ag nanoparticles embedded composite film. It shows the presence of Si, W, O, C and Ag elements. The concentration of Ag is found to be 12%. The high resolution spectrum of Ag 3d is given in Fig. 7b. The obtained binding energy values of the Ag $3d_{3/2}$ and $3d_{5/2}$ are 375.0 eV and 368.8 eV, respectively. The binding energy for metallic Ag foil is 374.50 and 367.18 eV. The Ag embedded composite film showed

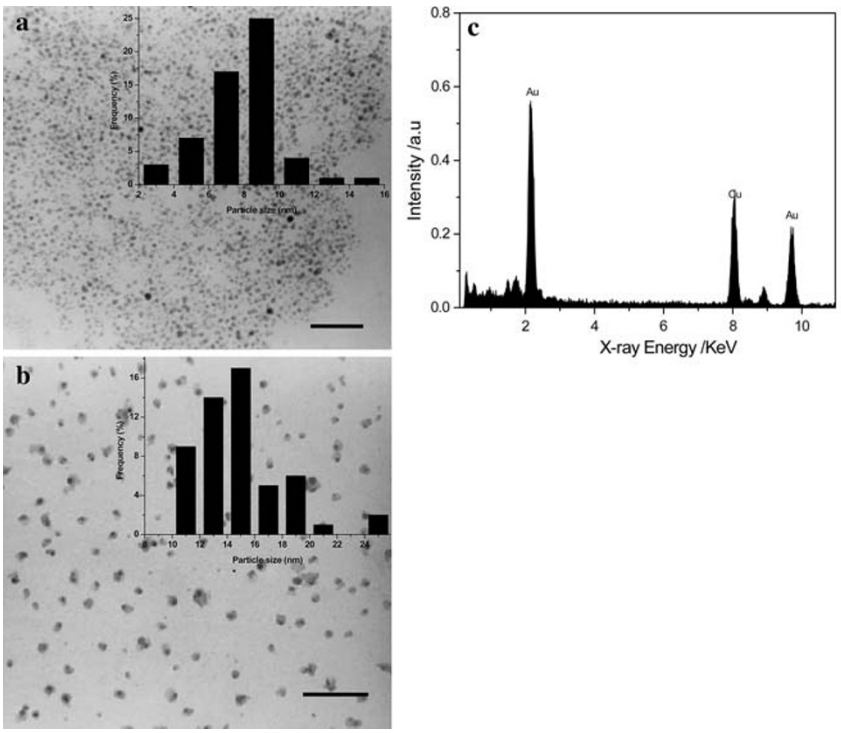

Fig. 6 TEM images of Au embedded composite films prepared with (**a**) 3.3 mM, (**b**) 5.4 mM $HAuCl_4$ and (**c**) EDX spectrum of (**b**). Inset shows corresponding histograms. Scale bar: 100 nm

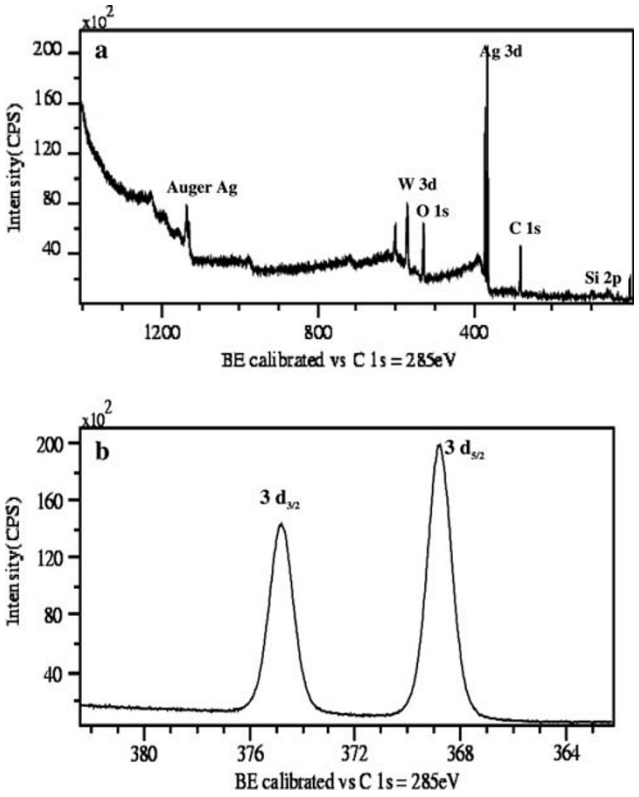

Fig. 7 XPS spectra of Ag embedded composite films (**a**) survey scan and (**b**) high-resolution spectra of Ag 3d

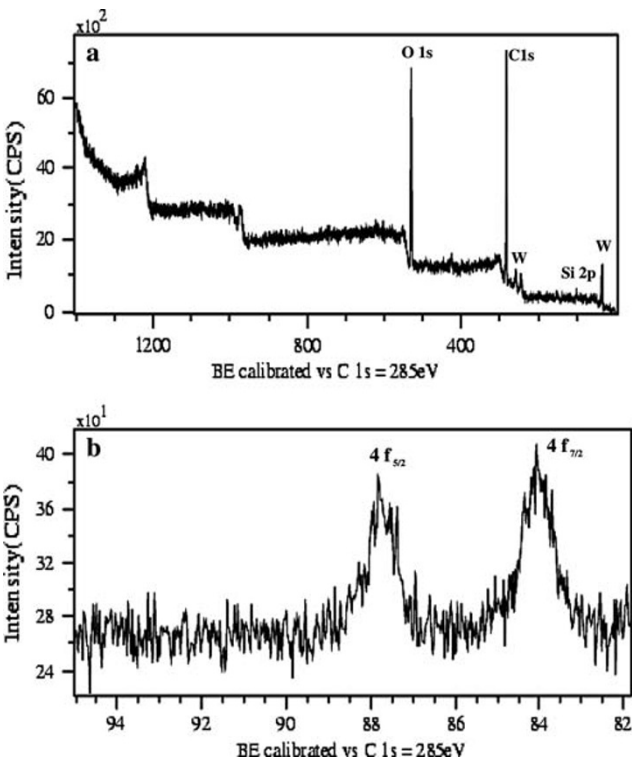

Fig. 8 XPS spectra of Au embedded composite film (**a**) survey scan and (**b**) high-resoltuion scan of Au 4f

higher B.E values compared to that of metallic bulk Ag foil. The binding energy shift (ΔE) with respect to the Ag foil is 0.65 eV. Shin et al. observed a binding energy shift of 0.7 and 1.4 eV, respectively for Ag particle size of 12.1 and 19.6 nm [30]. In the present study we observed 0.65 eV BE shift for 19 nm Ag particles. The positive shift of binding energy may be due the particle size, chemical, and charging effects [30]. The size effect is due to the change in electronic structure that results from changes in the boundary conditions with changes in the size of the nanoparticles. The chemical effect on the binding energy is due to the adsorption of polymer or silica onto the nanoparticles. In the present system, the Ag nanoparticles are bound to the different chemical species. XPS studies of Au embedded composite film (Fig. 8a) showed the presence of Si, W, O, C, and Au elements. The atomic concentration of Au is 5.6%. The BE values of Au $4f_{7/2}$ (84.1 eV) and Au $4f_{5/2}$ (87.9 eV) in Au embedded nanoparticles are higher when compared to the bulk Au foil. The positive shift of the BE energy of nanoparticles with respect to that of bulk metal is consistent with that reported in literature [31].

The photoluminescence of silver and gold metals is generally attributed to electronic transitions between the highest d band and conduction sp band. The composite containing Ag nanoparticles showed an emission band at 481 nm when excited at 435 nm (Fig. 9a). In order to corroborate whether the fluorescence emission is from the embedded Ag nanoparticles or from the parent compound, we have measured fluorescence for the composite without Ag nanoparticles (Fig. 9). The absence of band at this region indicates that the fluorescence emission is originating from the Ag nanoparticles. Henglein et al. observed luminescence from Ag nanoparticles reduced in the presence of polymers [32]. Zheng et al. observed fluorescence emission for dendrimer-encapsulated silver nanodots [33]. Ag nanoparticles stabilized by [poly(styrene)]-dibenzo-18-crown-6-[poly(styrene)] in solutions showed an emission band at 486 nm upon excitation at 408 nm [34]. The observed emission at 486 nm is attributed to the Ag nanoparticles. When the dipping time of composite film is increased, the intensity of the band at 481 nm increased which might be due to the increase in the amount of Ag (Fig. 9b). When increasing the concentration of the metal nanoparticles in composite film the intensity of emission peak also increased indicating the possible formation of complexing effect between the metal nanoparticles with polymer. The observation indicates that the matrix environment of composite improved the photoluminescence property of embedded silver nanoparticles due to the complexing effect between the functional groups of polymer. Figure 10a and b shows the excitation as well as the emission spectra of Au embedded composite film. The fluorescence emission band at 612 nm is due to the Au

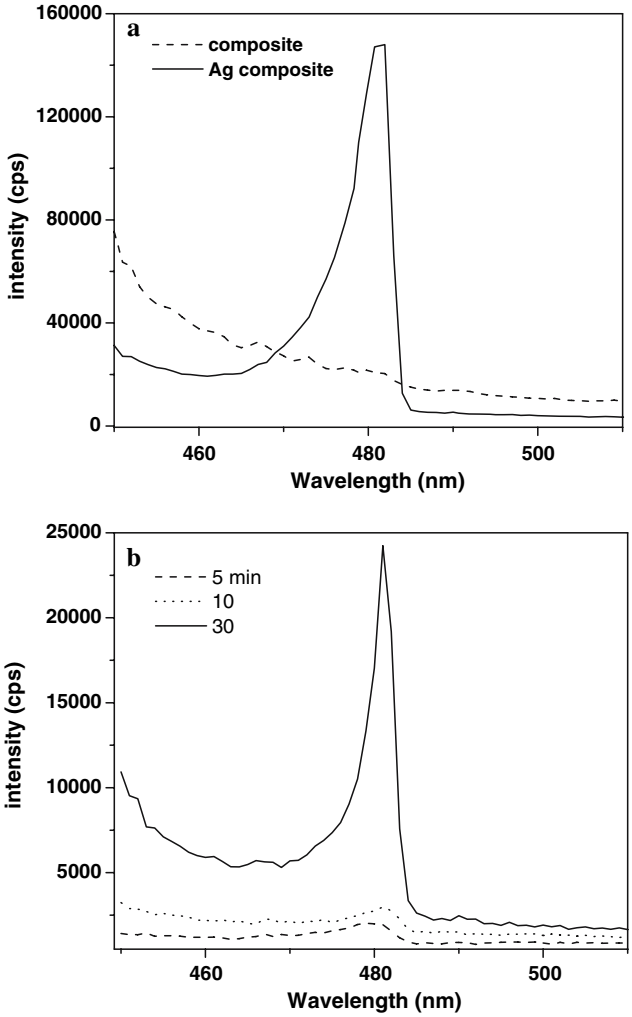

Fig. 9 Photoluminescence emission spectra of (**a**) composite with and without Ag nanoparticles ($\lambda_{Exc.}$ = 420 nm) and (**b**) composite film dipped for various time intervals (5, 10, and 30 min) in 20 mM $AgNO_3$

nanoparticles. The observed emission from Au nanoparticles is consistent with the reports of Geddes et al. [35]. The optical and fluorescence studies suggest that the noble metal embedded composite films can be used for optical devices such as optical filter etc., and the desired optical properties can be achieved by proper tuning the reaction parameters.

The formation of Ag or Au nanoparticles in the composite film can be attributed to the transfer of electrons from the photoreduced silicotungstate ion to Ag^+ or Au^{3+} ions thus leading to zero valent metallic state. The Ag^+ ions from solution diffuse inside or on the film matrix where it is reduced to Ag metal nanoparticles and the silicotungstate ions are reoxidized. The photo reduced $SiW_{12}O_{40}^{5-}$ is capable of transferring the electrons to the Ag^+ ions, thus Ag nanoparticles formed in the composite film. The first reduction potential of $SiW_{12}O_{40}^{4-}/SiW_{12}O_{40}^{5-}$ is 0.057 V vs NHE.

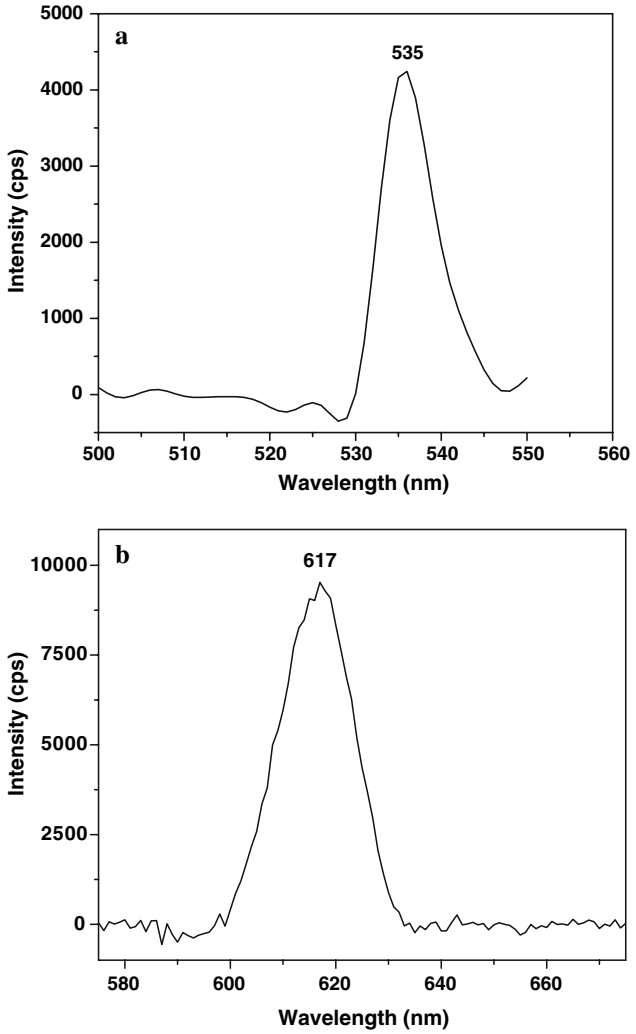

Fig. 10 Photoluminescence spectra of Au embedded composite film (**a**) excitation spectra ($\lambda_{Em.} = 617$) and (**b**) emission spectra ($\lambda_{Exc} = 535$ nm)

$$SiW_{12}O_{40}^{4-} + PVA \rightarrow SiW_{12}O_{40}^{5-} \quad (1)$$

$$SiW_{12}O_{40}^{5-} + M^{+} \rightarrow SiW_{12}O_{40}^{4-} + M^{0} \quad (\text{where } M^{+} \text{can be } Ag^{+},\ Au^{3+}) \quad (2)$$

The reduction potentials of Ag^{+}/Ag^{0}, Au^{3+}/Au^{0} is 0.799 and 1.002 V vs NHE. So the above reaction is thermodynamically favorable, thus the formation of Ag, Au nanoparticles was achieved easily by the present strategy. We have observed that the formation of Ag nanoparticles is very facile because the diffusion of Ag^{+} is higher than that of Au^{3+} and also due to hydrophilic nature of Ag [36]. Spontaneous self-assembly of silicotungstate anions on Ag (111) and Ag (100) are known [37]. Upon embedding the silicotungstate ion the composite, the first one electron reduction potential is shifted to more negative values. In the composite the one electron reduction potential of $[SiW_{12}O_{40}]^{4-}/[SiW_{12}O_{40}]^{5-}$ is –0.096 V vs NHE (parent couple 0.057 V). This enhancement of the reducing behavior also favors the facile formation of silver nanoparticles. The reaction in Equation (2) proceeds, within seconds at room temperature, utilizing a mild reductant, $[SiW_{12}O_{40}]^{5-}$. Whereas other reductive methods that proceed promptly at room temperature use rather strong reductants such as BH_{4}^{-}, hydrogen atoms, or organic radicals. On the other hand, conventional processes that use mild reducing agents often need heat to enable them to proceed within minutes or days. Controlled experiments were demonstrated that the silicotungstate ions are necessary for the rapid reduction of metal nanoparticles in composite films. We have also prepared other noble metal nanoparticles (Pd, Pt) using this strategy.

Conclusions

A simple and elegant method is described to embed silver and gold nanoparticles in organic-inorganic nanocomposite films. The embedded metal nanoparticles in composite films have been characterized with various physico-chemical techniques such as UV–Visible, TEM, EDAX and XPS. The composite film embedded with Ag nanoparticles is golden yellow in color and Au embedded composite film has pink color. The rate of formation of Ag nanoparticles is higher than that of Au nanoparticles. The surface plasmon band position, and the intensity shifts as the particle size and population increases. The optical properties of composite materials were attributed to the embedded metal nanoparticles. The emission of silver and gold nanoparticles composite films are attributed to the embedded metal nanoparticles. The adopted method demonstrates that the sizes of nanoparticles are of narrow size distribution and are highly distributed in the composite film. The composite film embedded with Ag nanoparticles is golden yellow in color and Au embedded composite film has a pink color. The rate of formation of Ag nanoparticles is higher than the Au nanoparticles. The surface plasmon band position, the half width and the intensity change with the particle size. The optical behavior of composite films was modulated using the dipping time intervals and concentration of the metal ion solutions. The size of particles is in the range of 10–20 nm for dipping time of 5–30 min. Homogeneous dispersion of metal nanoparticles is achieved, which can seen from TEM studies. As the dipping time increases the population of metal nanoparticles increased. It is evidenced from XRD and XPS analysis that the embedded metal nanoparticles are in zero valent state. The adopted synthetic procedure is amenable to fine-tune the properties of the composite film by choosing the suitable constituents at molecular level.

References

1. S. Foster, M. Antonietii, Adv. Mater. **10**, 195 (1998); R.P. Andres, J.C. Bielefeld, J.I. Henderson, D.B. Janes, V.R. Kolagunta, C.P. Kubiak, W.J. Mahoney, R.G. Osifchinm, Science **273**, 1690 (1996); A.P. Alivasators, Science **271**, 933 (1996)
2. H. Hirai, H. Wakabayashi, M. Komiyama, Chem. Lett. **1047**, 1983 (1983); K. Ghosh, S.N. Maiti, J. Appl. Polym. Sci. **60**, 323 (1996)
3. J.M. Thomas, Pure Appl. Chem. **60**, 1517 (1988)
4. J.A.A.J. Perenboom, P. Wyder, P. Meier, Phys. Rep. **78**, 173 (1981)
5. K.J. Klabunde, Nanoscale Materials in Chemistry, (Wiley Interscience, New York, 2001)
6. T.S. Ahmadi, Z.L. Wang, T.C. Green, A. Henglein, M.A. El-Sayed, Science **272**, 1924 (1996); P.Y. Silvert, R.H. Urbina, N. Duvauchelle, V. Vijayakrishnan, K.T. Elhsissen, J. Mater. Chem. **6**, 573 (1996)
7. P.V. Kamat, J. Phys. Chem. B **106**, 7729 (2002); Y. Zhou, C.Y. Wang, Y.R. Zhu, Z.Y. Chen, Chem .Mater. **11**, 2310 (1999)
8. W.X. Tu, H.F. Lin, Chem. Mater. **12**, 564 (2000)
9. Y. Mizukoshi, R. Oshima, Y. Maeda, Y. Nagata, Langmuir **15**, 2733 (1999)
10. A. Henglein, M. Giersig, J. Phys. Chem. B. **103**, 9533 (1999)
11. F. Stellacci, C.A. Bauer, T. Meyer-Friedrichen, W. Wenseleers, V. Alain, S.M. Kuebler, S.J. Pond, Y. Zhang, S.R. Marder, J.W. Perry, Adv. Mater.**14**, 194 (2002)
12. G.B. Smith, C.A. Deller, P.D. Swift, A. Gentle, P.D Garrett, W.K. Fisher, J. Nanopart. Res.**4**, 157 (2002)
13. I.-W. Park, M. Yoon, Y.M. Kim, Y. Kim, H. Yoon, H.J. Song, V. Volkov, A. Avilov, Y.J. Park, Solid State Commun. **126**, 385 (2003)
14. F.P. Zamborini, M.C. Leopold, J.F. Hicks, P.J. Kulesza, M.A. Malik, R.W. Murray, J. Am. Chem. Soc. **124**, 8958 (2002); E.C. Walter, K. Ng, M.P. Zach, R.M. Penner, F. Favier, Microelectron. Eng. **61–62**, 555 (2002)
15. V.M. Rudoy, B.G. Ershov, N.L. Sukhov, O.V. Dement'eva, A.V. Zaitseva, A.F. Seliverstov, M.E. Kartseva, V.A. Ogarev, Colloid J. **64**, 755 (2002)
16. C. Aymonier, U. Schlotterbeck, L. Antonietti, P. Zacharias, R. Thomann, J.C. Tiller, S. Mecking, Chem. Commun. 3018 (2002); S. Shanmugam, B. Viswanathan, T.K. Varadarajan, Mater. Chem. Phys. **95**, 51 (2006)
17. V.M. Rudoay, B.G. Ershov, N.L. Sukhov, O.V. Dement'eva, A.V. Zaitseva, A.F. Seliverstov, M.E. Kartseva, V.A. Ogarev, Colloid J. **64**, 755 (2002)
18. Y. Zhang, F. Chen, J. Zhuang, Y. Tang, D. Wang, Y. Wang, A. Dong, N. Ren, N. Chem. Commun. 2814 (2002); Y. Zhou, H. Itoh, T. Uemura, K. Naka, Y. Chujo, Chem. Commun. 613 (2001); S.K. Mandal, R.K. Roy, A.K. Pal, J. Phys. D: Appl. Phys. **36**, 261 (2003); L. Yang, G.H. Li, J.G. Zhang, L.D. Zhang, Y.L. Liu, Q.M. Wang, Appl. Phys. Lett. **78**, 102 (2001); Y. Dirix, C. Bastiaansen, W. Caseri, P. Smith, J. Mater. Sci. **34**, 3859 (1999); L. Yang, G.H. Li, L.D. Zhang, Appl. Phys. Lett. **76**, 1537 (2000); G. Mitrikas, C.C. Trapalis, G. Kordas, J. Chem. Phys. **111**, 8098 (1999); T. He, A. Kunitake, O. Nakao, Chem. Mater.**15**, 4401 (2003)
19. M.T. Pope, Heteropoly and Isopoly Oxometalates, (Springer, Berlin, 1983)
20. M.T. Pope, A. Muller, Angew. Chem. **30**, 34 (1991)
21. M. Sadakane, E. Steckhan, Chem. Rev. **98** 219 (1998)
22. A. Troupis, A. Hiskia, E. Papaconstantinou, Angew. Chem. Int. Ed. **41**, 1911 (2002)
23. S. Mandal, P.R. Selvakannan, R. Pasricha, M. Sastry, J. Am. Chem. Soc. **125**, 8440 (2003)
24. S. Shanmugam, B. Viswanathan, T.K. Varadarajan, J. Mol. Catal. A **241** 52 (2005)
25. M.G. Vagara, E. Papaconstantinou, M.T. Pope, Inorg. Chem. **9**, 662 (1970)
26. S. Shanmugam, B. Viswanathan, T.K. Varadarajan, J. Member. Sci. **275**, 105 (2006)
27. Y. Dirix, C. Bastiaansen, W. Caseri, P. Smith, Adv. Mater.**11**, 223 (1999)
28. I. Hussian, M. Brust, A.J. Papworth, A.I. Cooper, Langmuir **19**, 4831 (2003)
29. U. Kreibig, M. Vollmer, Optical Properties of Metal Clusters, (Springer, Berlin, 1995)
30. H.S. Shin, H.C. Choi, Y. Jung, S.B. Kim, H.J. Song, H.J. Shin, Chem. Phys. Lett. **383**, 418 (2004)
31. G.K. Wertheim, S.B. Dicenzo, D.N.E. Buchanan, Phys. Rev. B. **33**, 5384 (1986);G.K. Wertheim, S.B. Dicenzo, S.E. Youngquist, Phys. Rev. Lett. **51**, 2310 (1983)
32. A. Henglein, T. Linnert, P. Mulvaney, Ber.der Bunsen-Gesellschaft **94**, 1449 (1990)
33. J. Zheng, R.M. Dickson, J. Am. Chem. Soc. **124**, 13982 (2002)
34. J. Gao, J. Fu, C. Lin, J. Lin, Y. Han, X. Yu, C. Pan, Langmuir **20**, 9775 (2004)
35. C.D. Geddes, A. Parfenov, I. Gryczynski, J.R. Lakowicz, Chem. Phys. Lett. **380**, 269 (2003)
36. G.W. Arnold, J.A. Borders, J. Appl. Phys. **48**, 1488 (1977)
37. L. Lee, J.X. Wang, R.R. Adzic, I.K. Robinsion, A.A. Gewirth, J. Am. Chem. Soc. **123**, 8838 (2001)